

# Precise synchronization of a free-running Rubidium atomic clock with the GPS Time **for applications in experimental particle physics**

Claire Dalmazzone<sup>1a</sup>, Mathieu Guigue<sup>a</sup>, Lucile Mellet<sup>2a</sup>, Boris Popov<sup>a</sup>,  
Stefano Russo<sup>a</sup>, Vincent Voisin<sup>a</sup>,  
Michel Abgrall<sup>b</sup>, Baptiste Chupin<sup>b</sup>, Caroline B. Lim<sup>b</sup>, Paul-Éric Pottie<sup>b</sup>,  
Pierre Ulrich<sup>b</sup>

<sup>a</sup>*Laboratoire de Physique Nucléaire et des Hautes Energies (LPNHE), Sorbonne Université, CNRS/IN2P3, 4 place Jussieu, Paris, 75005, France*

<sup>b</sup>*LNE-SYRTE, Observatoire de Paris, Université PSL, CNRS, Sorbonne Université, 61 avenue de l'Observatoire, Paris, 75014, France*

---

## Abstract

We present results of our study devoted to the development of a time correction algorithm needed to precisely synchronize a free-running Rubidium atomic clock with the Coordinated Universal Time (UTC). This R&D is performed in view of the Hyper-Kamiokande (HK) experiment currently under construction in Japan, which requires a synchronization with UTC and between its different experimental sites with a precision better than 100 ns. We use a Global Navigation Satellite System (GNSS) receiver to compare a PPS and a 10 MHz signal, generated by a free-running Rubidium clock, to the Global Positioning System (GPS) Time signal. We use these comparisons to correct the time series (time stamps) provided by the Rubidium clock signal. We fit the difference between Rubidium and GPS Time with polynomial functions of time over a certain integration time window to extract a correction of the Rubidium time stamps in offline or online mode. In online mode, the latest fit results are used for the correction until a new comparison to the GPS Time becomes available. We show that with an integration time window of around  $10^4$  seconds, we can correct the time stamps drift, caused

---

<sup>1</sup>Corresponding author: [claire.dalmazzone@lpnhe.in2p3.fr](mailto:claire.dalmazzone@lpnhe.in2p3.fr), +33617925827

<sup>2</sup>Now at Michigan State University, Department of Physics and Astronomy, East Lansing, Michigan, USA

by the frequency random walk noise and the deterministic frequency drift of the free running Rubidium clock, so that the time difference with respect to the GPS Time stays within a  $\pm 5$  ns range in both offline or online correction mode. **Presented results could be of interest for other experiments in the field of neutrino physics and multi-messenger astrophysics.**

*Keywords:* timing detectors, precise timing, atomic clock, GPS, UTC

*PACS:* 06.30. -k, 06.30.Ft, 07.05.Fb

*2000 MSC:* 00A79, 85-05, 85-08

---

## 1. Introduction

A precise synchronization with the Coordinated Universal Time (UTC) or with another signal is a necessity in many applications, particularly in long-baseline physics experiments spread over several experimental sites. A good example is long-baseline neutrino oscillation experiments, like OPERA [1] (2006-2012), T2K [2] (from 2010) and NOvA [3] (from 2014), where a beam of neutrinos is produced and characterized in a first experimental site and detected, after several hundreds of kilometers of propagation, at another site to measure a change of the beam properties. Two next generation long-baseline neutrino experiments are being built at the moment: Hyper-Kamiokande (HK) [4] that plans to start taking data in 2027 and DUNE [5, 6] that should begin sometime after 2029. These experiments require a synchronization of 100 ns or better between the different experimental sites. Moreover, multi-messenger programs that plan to compare different components of astrophysical events [7] (e.g.: gamma-ray bursts, gravitational waves, neutrino emissions of supernovae, etc.) require a synchronization with UTC of different experiments located all over the world. For instance, to enter the SuperNova Early Warning System (SNEWS) network [8], a synchronization to UTC better than 100 ns is required.

Many long-baseline physics experiments use atomic oscillators as frequency references because of their good short term stability. Among the reference oscillators available on the market, Rubidium atomic clocks are generally chosen for their affordability as it was the case for the T2K [9] and Super-Kamiokande [10] timing systems. However, Rubidium clocks usually drift away from a stable reference because of frequency drift and random walk. For synchronization to UTC, this drift usually needs to be prevented

27 or corrected. A common solution is to discipline the average frequency of  
28 the clock to the signals of an external Global Navigation Satellite System  
29 (GNSS) receiver, with an integration time window chosen so that it does not  
30 deteriorate the short term stability of the clock. However, it presents some  
31 drawbacks like the fact that the user has little control on the setup. In case  
32 of problems (like jumps in the time comparison), it is difficult to understand  
33 where they come from (GPS Time, receiver, the master clock, etc.) and  
34 to assess the uncertainty on the synchronization to UTC. The R&D work  
35 presented in this paper and introduced in [11] is focused on designing and  
36 characterizing an alternative method that allows more freedom to the user  
37 and a better understanding of the process. It is based on known metrology  
38 techniques [12, 13]. The proposed method uses a free-running atomic clock  
39 to derive a time signal and provide time stamps. In a physics experiment  
40 these would be the time stamps of detected events. The time stamps are  
41 corrected in post-processing using comparisons of the Rubidium clock signal  
42 to GNSS Time. In that way, we can store all the information (the raw signal,  
43 the comparisons to GPS Time, the derived correction etc.) and apply the  
44 correction in either online (during the data-acquisition) or offline modes. Let  
45 us note that the GNSS time is a good approximation of the UTC, within a  
46 few nanoseconds, and it allows synchronization to UTC via a common-view  
47 technique [14]. The common-view would be performed with a national labo-  
48 ratory providing a local realization of UTC(k), like e.g. the NICT laboratory  
49 in Japan [15]. Then the conversion to UTC can be performed with the help of  
50 the Circular T of the BIPM (Bureau International des Poids et Mesures) [16]  
51 at the end of each month.

## 52 **2. Materials and Methods**

### 53 *2.1. Experimental setup*

54 The experimental setup that we used is schematized in Figure 1. It is  
55 located at the Pierre and Marie Curie (Jussieu) campus of the Sorbonne  
56 University in Paris. The setup consists of two main parts: one represents  
57 the timing generation and correction setup, that could be reproduced in the  
58 HK experiment, and the second part is related to testing the efficiency of the  
59 correction method. In the first part a Rubidium clock (Rb) in free-running  
60 mode, at the ground floor of the laboratory, generates a Pulse Per Second  
61 (PPS) signal and a 10 MHz signal that are transported to the fifth floor with  
62 the White Rabbit (WR) protocol [17]. The timing signals of the slave WR

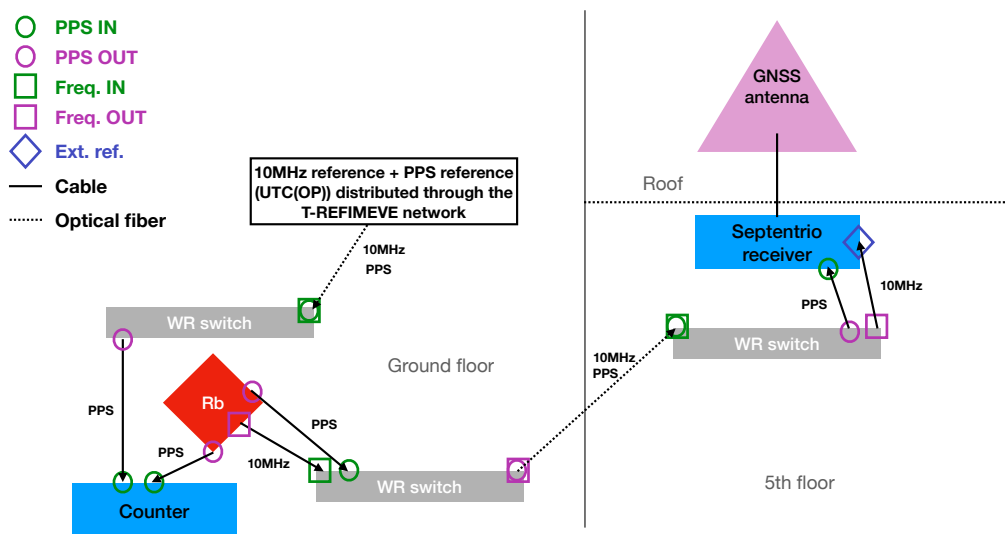


Figure 1: Experimental setup used in this work. Part of the equipment is installed at the ground floor and the other part at the fifth floor. The relevant signals generated at the ground floor are transported to the fifth floor via optical fibers with the White Rabbit (WR) protocol. This particular setup mimics what could happen in underground experiments where the clock signal would be generated underground whereas the GNSS antenna and receiver would be located above-ground.

63 switch are used by a GNSS receiver as a reference for its internal clock. The  
64 receiver connected to its antenna on the roof, above the fifth floor, is used to  
65 measure time comparisons between the GPS Time and the Rubidium clock.  
66 This physical distance between the time generation part and the receiver was  
67 done on purpose to mimic what would happen in many long-baseline physics  
68 experiments. Indeed, in Hyper-Kamiokande, the Rubidium clock would be  
69 placed inside a mountain, where a cavern has been dug to host the detector,  
70 whereas the receiver would have to be placed outside in a valley. The second  
71 part of our experimental setup is contained in the experimental room at the  
72 ground floor and its purpose is to validate the performance of the method  
73 and would thus not be reproduced in the final setup in Hyper-Kamiokande.  
74 It consists of a counter measuring the time difference between the Rubidium  
75 clock PPS signal and the French realization of UTC (called UTC(OP) for  
76 Observatoire de Paris). The UTC(OP), as well as a 10 MHz reference signal,  
77 are available at the laboratory, as part of the T-REFIMEVE network [18, 19],  
78 via a third White Rabbit switch.

#### 79 *2.1.1. Rubidium clock*

80 The Rubidium atomic clock used is the FS725 Rubidium Frequency Stan-  
81 dard sold by Stanford Research Systems integrating a rubidium oscillator of  
82 the PRS10 model. It provides two 10 MHz and one 5 MHz signals with low  
83 phase white noise and its stability estimated via the Allan Standard Devi-  
84 ation (ASD) [20] at 1 s is about  $2 \times 10^{-11}$ . It also provides a PPS output  
85 with a jitter of less than 1 ns. Its 20 years aging was estimated to less than  
86  $5 \times 10^{-9}$  and the Mean Time Before Failure is over 200,000 hours. In this  
87 work we use the Rubidium clock in free-running mode but it can also be  
88 frequency disciplined using an external 1 PPS reference, based on GPS for  
89 instance. The FS725 is installed at the ground floor of our laboratory and  
90 its 10 MHz and 1 PPS outputs are transported to the GNSS receiver at the  
91 fifth floor.

#### 92 *2.1.2. White Rabbit switches*

93 The White Rabbit (WR) project [17] is a collaborative effort involving  
94 CERN, the GSI Helmholtz Centre for Heavy Ion Research, and other part-  
95 ners from academia and industry. Its primary objective is to develop a highly  
96 deterministic Ethernet-based network capable of achieving sub-nanosecond  
97 accuracy in time transfer. Initially, this network was implemented for dis-  
98 tributing timing signals for control and data acquisition purposes at CERN's

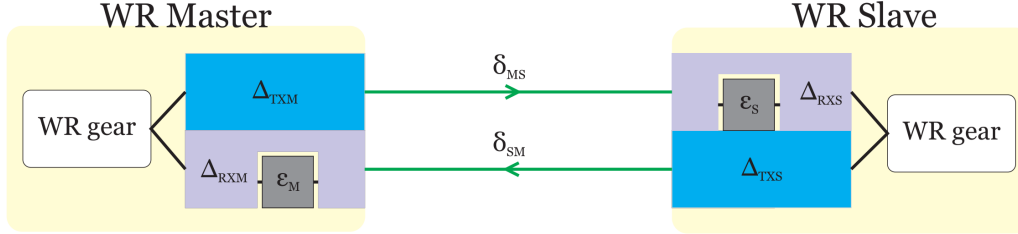


Figure 2: White Rabbit link model, from [21]

99 accelerator sites. The described experimental setup uses two WR switches  
 100 to propagate with great precision the Rubidium clock PPS and frequency  
 101 signals from the ground floor to the fifth floor.

102 The calibration of the link allows to obtain a sub-nanosecond synchrono-  
 103 zation between switches. A White Rabbit link between two devices is char-  
 104 acterized by specific hardware delays and fiber propagation latencies. Each  
 105 WR Master and WR Slave possesses fixed transmission and reception delays  
 106 ( $\Delta T_{XM}$ ,  $\Delta RXM$ ,  $\Delta T_{XS}$ ,  $\Delta RXS$ ). These delays are the cumulative result  
 107 of various factors such as SFP transceiver, PCB trace, electronic component  
 108 delays, and internal FPGA chip delays. Additionally, there is a reception  
 109 delay on both ends caused by aligning the recovered clock signal to the inter-  
 110 symbol boundaries of the data stream, referred to as the bitslide value ( $\epsilon_M$   
 111 and  $\epsilon_S$  in Figure 2). We can see the results of calibration process using a  
 112 counter in Figure 3, the difference of PPS signals between the WR slave and  
 113 master switches changes from 165 ps to 60 ps (with a 100 m long fiber).  
 114 Delays introduced by the cables were subtracted to the mean values.

115 As a part of the T-REFIMEVE network [18, 19], the LPNHE has ac-  
 116 cess through a dedicated switch to the official French realization of the  
 117 UTC, called UTC(OP) (for Observatoire de Paris) [22], transported from  
 118 the SYRTE laboratory via White Rabbit protocol. REFIMEVE is a French  
 119 national research infrastructure aiming at the dissemination of highly ac-  
 120 curate and stable time and frequency references to more than 30 research  
 121 laboratories and research infrastructures all over France. The reference sig-  
 122 nals originate from LNE-SYRTE and are mainly transported over the optical  
 123 fiber backbone of RENATER, the French National Research and Education  
 124 Network.

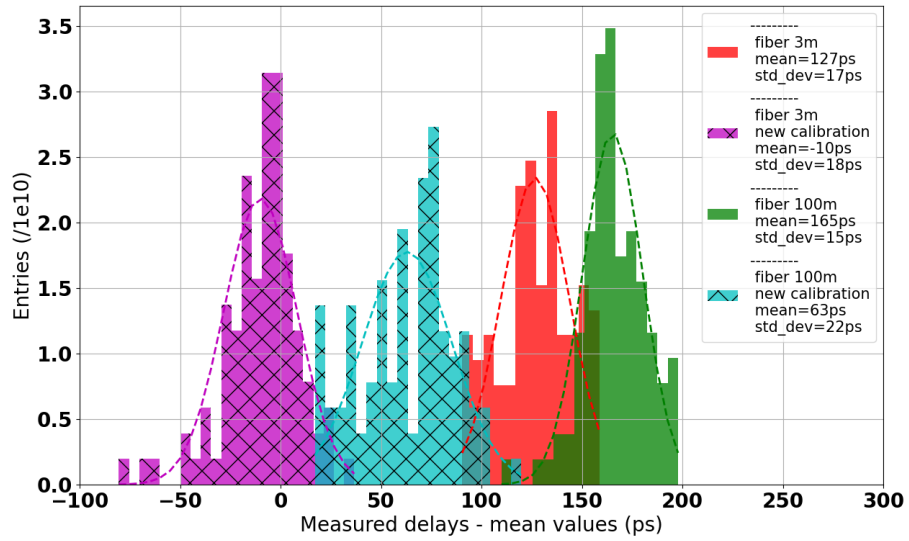
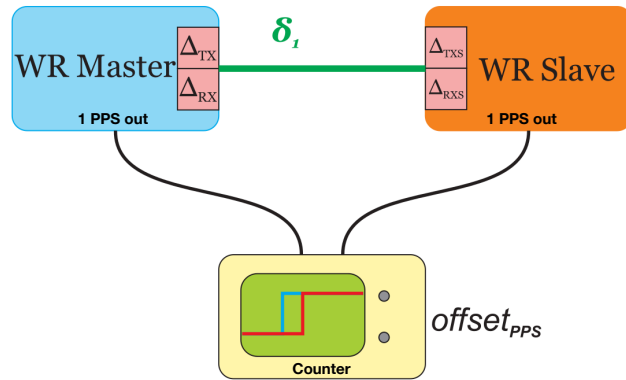


Figure 3: Difference between the PPS OUT signals of the White Rabbit slave and master switches before and after calibration

125 *2.1.3. Counter*

126 The counter is the 53220A model from Keysight Technologies. Here it  
127 was used to measure the time interval between the two PPS signals: the  
128 UTC(OP) PPS reference and the one generated by the free-running Rubid-  
129 ium clock. The input channel(s) are (by default) configured for auto-leveling  
130 at 50% with a positive slope.

131 *2.1.4. Septentrio GNSS antenna and receiver*

132 We use the Septentrio PolaNt Choke ring GNSS antenna that supports  
133 GNSS signals from many satellite constellations including GPS, GLONASS,  
134 Galileo and BeiDou. In this work, we restrict the analysis to GPS but it  
135 can easily be generalized to any subset of constellations. The antenna po-  
136 sition has been previously measured to a precision better than 6 mm by  
137 trilateration with the help of a web-based service provided by the Canadian  
138 government [23]. We use a Septentrio PolaRx5 GNSS reference receiver as a  
139 timing receiver to compare GPS Time to the Rubidium clock. The receiver  
140 performs measurements based on the 10 MHz reference signal coming via  
141 White Rabbit from the Rubidium clock. The Rubidium clock 1 PPS signal  
142 is also transported to the receiver via White Rabbit to allow, at initializa-  
143 tion, to identify the 10 MHz cycle. Note that this 1 PPS input is kept during  
144 the whole data-taking to avoid possible phase jumps due to perturbations.  
145 The Septentrio receiver provides one measurement every 16 min which is the  
146 middle point of the linear function fitted from the 13 min of data from the  
147 beginning of this 16 min time window. The results of the measurements are  
148 registered using the CGGTTS file format [24].

149 Before taking measurements, the whole system has been calibrated against  
150 official reference signals from the SYRTE laboratory. As it can be seen in  
151 Figure 4, the following delays need to be measured and taken into account  
152 during operation [25]. The calibration procedure [26] consists in measuring  
153 these:

- 154 •  $X_S$ : internal delay inside the antenna, frequency dependent
- 155 •  $X_C$ : delay caused by the antenna cable
- 156 •  $X_R$ : internal delay of the receiver for the antenna signal, frequency  
157 dependent
- 158 •  $X_P$ : in case an external signal is given in input, connection cable delay



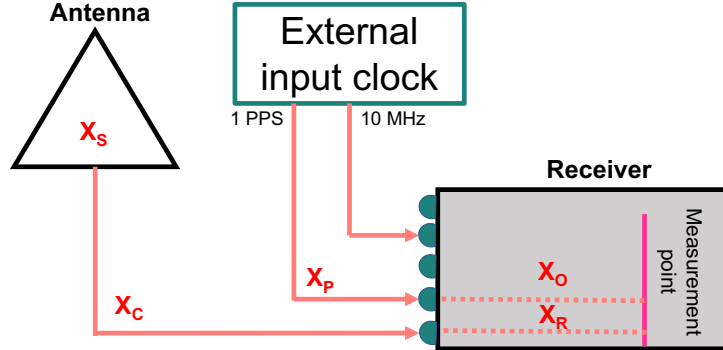


Figure 4: Delays to consider for the selected GNSS receiver+antenna pair, from [27]

- 159 •  $X_O$ : in case an external signal is given in input, internal receiver delay  
160 between external 1 PPS and internal clock

161  $X_S$  and  $X_R$  depend on the GNSS carrier frequency that is being tracked,  
162 meaning it is specific to each frequency of each GNSS constellation. The cal-  
163 ibration was performed for both GPS and Galileo constellations, each having  
164 two available carrier frequencies. The cable delays  $X_C$  and  $X_P$  were evaluated  
165 with an oscilloscope by sending a pulse in the cable and measuring the timing  
166 of the reflection. To reproduce the experimental conditions of underground  
167 experiments like HK or DUNE where the GPS antenna is outside, away from  
168 the detector, a 100 m cable was used and calibrated. The total cable delay  
169 was measured to be 505 ns. The internal delays of the antenna and receiver  
170 can only be measured together (for each frequency) as  $INTDLY = X_S + X_R$ .  
171 This was done through a comparison with OP73, one of the calibrated GNSS  
172 stations of SYRTE, and with UTC(OP), the French realization of UTC, as  
173 an input to the two receivers. The values of INTDLY found for the two most  
174 widely available carrier frequencies of the GPS constellation (L1 and L2) and  
175 the Galileo constellation (E1 and E5a) are given in Table 1.

176

177 The delays  $X_C$ , INTDLY, and REFDLY can then be given as parameters  
178 of the receiver so that they are automatically handled in any further use of  
179 the receiver. Uncertainties on the measured delays were evaluated to 4 ns ac-  
180 cording to estimations fixed for the employed method. The calibration needs  
181 to be re-done for any new antenna+receiver+antenna cable combination.

Table 1: Values of INTDLY in ns found for the first antenna+receiver system calibrated at the SYRTE laboratory against the OP73 station

GPS L1	GPS L2	Galileo E1	Galileo E5a
25.832	22.871	28.242	25.431

182 *2.2. Corrections methods*

183 *2.2.1. General principle*

184 To synchronize the Rubidium time stamps to UTC, we apply a time-  
 185 dependent correction (quadratic or linear) to the time series generated by  
 186 the free-running Rubidium clock  $\phi_{Rb}(t)$ . We model the  $k^{\text{th}}$  portion of the  
 187 time series ( $dt_{Rb,GPS}$ ), defined as the difference between the free-running  
 188 Rubidium clock and the GPS Time, as a (one or two degrees) polynomial of  
 189 time

$$\forall t \in [t_{k-1}, t_k], dt_{Rb,GPS}(t) = a_k \cdot t^2 + b_k \cdot t + c_k. \quad (1)$$

190 The coefficients  $a_k$  ( $a_k = 0$  in case of linear fit),  $b_k$  and  $c_k$  of the polynomials  
 191 are extracted from least square polynomial fits of the time difference distri-  
 192 butions. The fits of these differences, obtained from the Septentrio receiver,  
 193 are performed for every  $k^{\text{th}}$  time window of length  $\Delta t$ . In other words, we  
 194 model the Septentrio measurements with a piece-wise polynomial function of  
 195 time. For the  $k^{\text{th}}$  time window (between  $t_k$  and  $t_{k+1}$ ), we get the corrected  
 196 time stamps

$$\forall t \in [t_k, t_{k+1}], \phi_{Rb,corr}(t) = \phi_{Rb}(t) - a_k \times t^2 - b_k \times t - c_k. \quad (2)$$

197 The time-length  $\Delta t$  of the pieces (time windows) has to be chosen carefully.  
 198 In particular, it should be short enough in order to correct for the effect of  
 199 the frequency random walk of the Rubidium clock.

200 In the following, we consider two types of correction: the offline and the  
 201 online corrections. The difference between the two methods is illustrated in  
 202 Figure 5. The offline correction consists in using the Septentrio data from  
 203 the same time-window as the Rubidium signal to extract the  $a_k$ ,  $b_k$  and  $c_k$   
 204 coefficients. This correction is called offline because it requires the Septentrio  
 205 data from up to  $t_k + \Delta t = t_{k+1}$  to correct all the time stamps between  $t_k$  and  
 206  $t_{k+1}$  so it cannot be performed in real-time (one would need to wait a time  
 207  $\Delta t$  to extract the correction coefficients for the  $t_k$  time stamp).

208 The online correction consists in correcting the Rubidium time stamps  
 209 between  $t_k$  and  $t_{k+1}$  using Septentrio data collected before  $t_k$ . One example

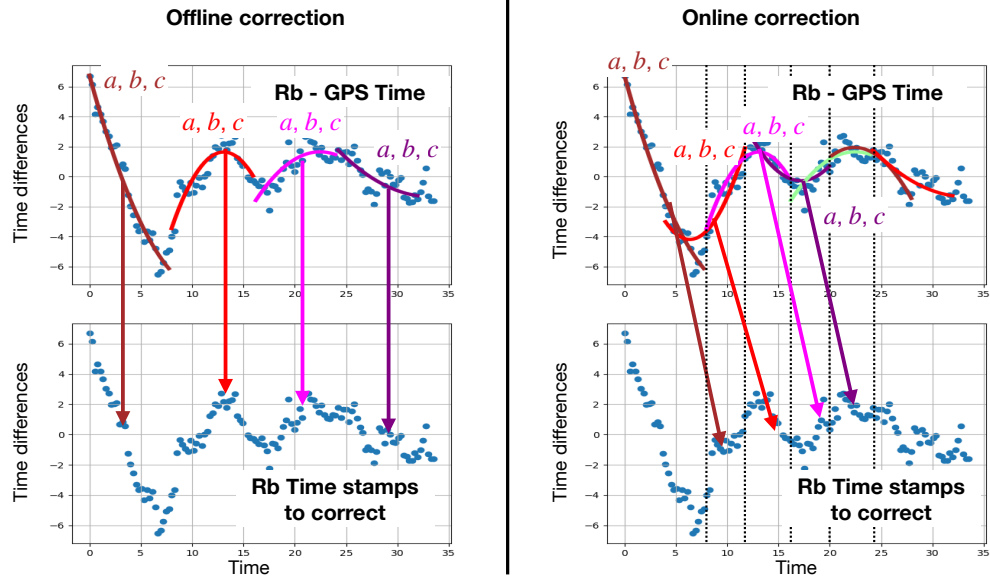


Figure 5: Schematic representation of the offline (left) and online (right) corrections. In the offline correction, we extract the correction coefficients using Rubidium - GPS Time comparison from the same time-window as the data we want to correct. In the online correction, we use Rubidium - GPS Time comparison from the previous time-window with respect to the data interval we want to correct. Only the second correction can be applied in real time as it only requires comparisons with GPS Time from previous measurements.

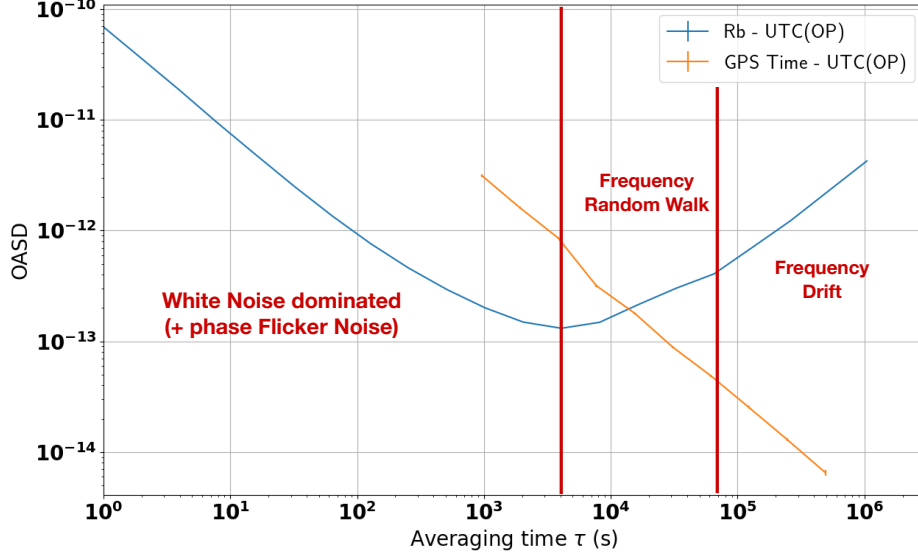


Figure 6: Overlapping Allan Standard Deviation of the Rb vs UTC(OP) time difference (in blue), measured by the counter, before any correction, and of GPS Time vs UTC(OP) (in orange) measured by the Septentrio receiver. The main types of noises affecting the Rubidium clock stability are indicated where they are limiting the stability.

210 of online correction is illustrated in Figure 5 where overlapping windows are  
 211 used. This method is called online because it can be applied in real time.  
 212 In the following, we will consider the most frequent possible update of the  
 213  $a_k$ ,  $b_k$  and  $c_k$  coefficients: they will be updated every time we receive a new  
 214 data point from the Septentrio receiver (every  $\delta t \approx 16$  minutes in our case).  
 215 This means that we have  $t_{k+1} = t_k + \delta t$  so that the  $a_k$ ,  $b_k$  and  $c_k$  coefficients  
 216 are extracted using Septentrio data between  $t_k - \Delta t$  and  $t_k$  and are used  
 217 to correct the time stamps between  $t_k$  and  $t_k + \delta t$ . In that particular case  
 218 every Septentrio data point will have been used in multiple fits, the number  
 219 depending on the length of the fit time window  $\Delta t$ .

220 The performance of the correction is evaluated in two ways. First, we look  
 221 at the stability of the corrected time series estimated with the Overlapping  
 222 Allan Standard Deviation (OASD). Then, we also look at the time difference  
 223 against GPS signal after correction.

224 *2.2.2. Validation of the method with simulations*

225 Before evaluating the performance of our timing system when integrating  
 226 the correction algorithm, the method was validated on simulated signals [27]  
 227 in order to isolate the effect and performance of the correction from any  
 228 measurement issues.

229 ***Simulation details.*** Three types of signals were considered: a perfect clock  
 230 to be used as a reference to evaluate the performance, a free-running Rubid-  
 231 ium clock and a GPS time signal, as measured by the Septentrio receiver.  
 232 The quadratic drift was not included because it is deterministic and is there-  
 233 fore not challenging to correct. At first order, the clock signal can be modeled  
 234 by white noise ( $WN$ ) in both phase and frequency as well as a random walk  
 235 ( $RW$ ) noise in frequency. Based on the characterization of the Rubidium  
 236 clock, the phase and frequency flicker noises can be neglected for this pur-  
 237 pose. Indeed, the characterization of our Rubidium clock in Figure 6 showed  
 238 that the frequency flicker noise had a negligible impact on the OASD. Fur-  
 239 thermore, the phase white and flicker noises have a similar impact on the  
 240 standard OASD and cannot be distinguished here. We chose to ignore the  
 241 phase flicker noise as it is less straightforward to simulate and it should not  
 242 impact the long term random walk drift that we want to correct. The GPS  
 243 Time can be modeled as pure phase white noise. The corresponding OASD  
 244 as a function of the averaging time  $\tau$  can be modeled [28, 29, 30] by:

$$OASD(\tau) \cong A_{WNp} \times \tau^{-1} + A_{WNf} \times \tau^{-1/2} + A_{RWf} \times \tau^{+1/2}. \quad (3)$$

245 The amplitudes  $A$  of these main frequency and phase noises were determined  
 246 through fitting this model (Eq. 3) to the OASD of the data when character-  
 247 izing our equipment (see Figure 6) and found to be:

$$\begin{aligned} A_{WNf} &= 7 \times 10^{-12} \text{ s}^{1/2}, \\ A_{RWf} &= 1 \times 10^{-15} \text{ s}^{-1/2}, \\ A_{WNp} &= 5 \times 10^{-11} \text{ s}, \end{aligned} \quad (4)$$

248 for the free-running Rubidium clock and for the GPS Time:

$$\begin{aligned} A_{WNf} &= 0 \text{ s}^{1/2}, \\ A_{RWf} &= 0 \text{ s}^{-1/2}, \\ A_{WNp} &= 2 \times 10^{-9} \text{ s}, \end{aligned} \quad (5)$$

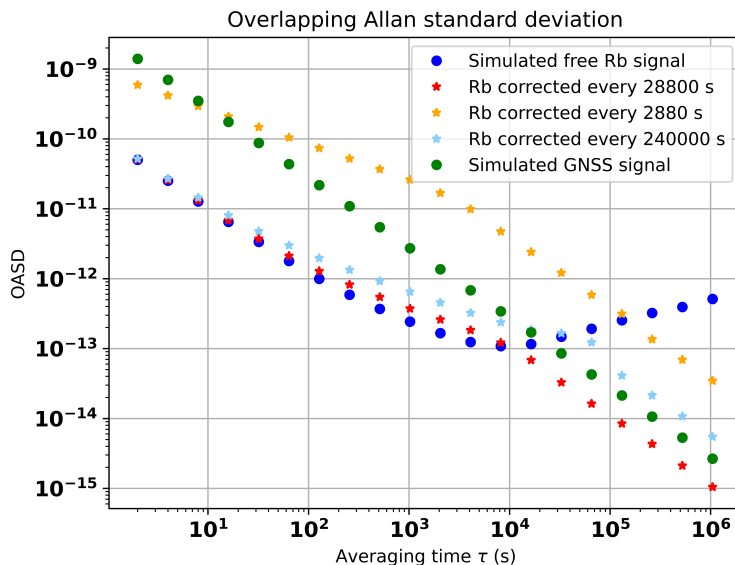


Figure 7: Comparison of overlapping ASD for corrected signals, with offline correction, with different time windows

249 with indices  $f$  and  $p$  for frequency and phase respectively. Using random  
 250 numbers generation and a model with these types of noise discussed just  
 251 above, time series were simulated.

252 The equivalent of  $10^6$  s of data was simulated. To mimic the output of  
 253 the GNSS receiver, time differences between the simulated Rubidium clock  
 254 and the simulated GPS Time ( $\Delta t_{Rb-ref}^i$ ) are computed every 16 mn.

255 **Offline corrections.** First, the offline corrections were tested on the sim-  
 256 ulated data. In Figure 7, the uncorrected simulated signals of the GPS and  
 257 the clock are reported in dotted symbols for comparison. The increase of  
 258 the clock's OASD after  $\tau = 10^4$  s due to the random walk is clearly visible.  
 259 One can see that with the OASD of the signals (starred symbols) that the  
 260 correction do eliminate the random walk at longer terms which indicates a  
 261 success of the method (quadratic). Moreover, one can determine that the  
 262 ideal length  $\Delta t$  of the correction time windows lies around  $3 \times 10^4$  s which  
 263 corresponds logically to the intersection of the free-running Rubidium clock  
 264 and GPS Time OASD curves. Indeed, the red curve with a time window of  
 265 28800 s shows an ideal combination of the short-term stability of the clock

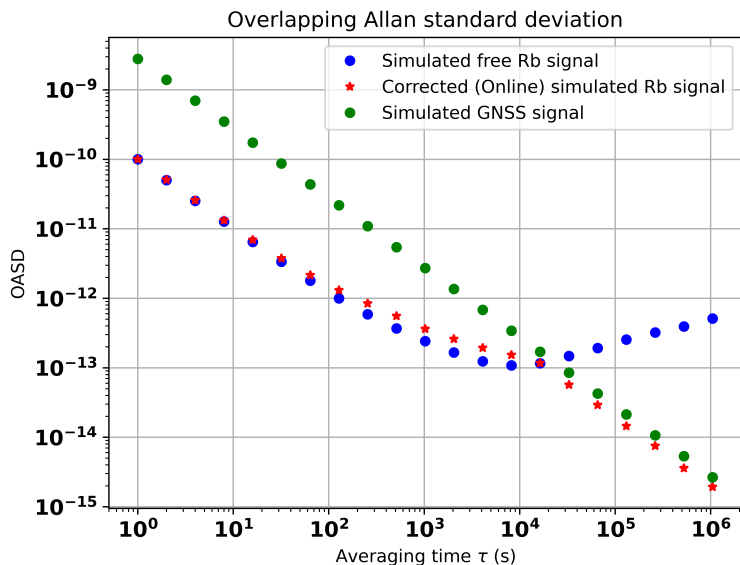


Figure 8: After online corrections at  $3 \times 10^4$  s: Overlapping ASD with respect to perfect signal

266 and the absence of random walk at longer scales. On the opposite, the yellow (shorter time window) and light blue (longer time window) curves show  
 267 respectively a degradation of the short term performance and a remaining  
 268 random walk component in the region between  $\tau = 10^4$  s and the time window  
 269 length (here 240000 s).  
 270

271 **Online corrections.** The online (linear) correction method was then applied to the simulated data using time series directly and a correction window  
 272 length of  $\Delta t = 3 \times 10^4$  s. The results are shown in Figure 8 in red and  
 273 prove to be just as efficient as the offline correction method to remove the  
 274 random walk at longer time scales which is the main goal. The overall precision on the long term region (after  $\approx 10^3$  s) is as expected slightly degraded  
 275 compared to the offline correction.  
 276  
 277

278 **Conclusion on simulation.** As a conclusion, it can be said that the application of the correction algorithms to the simulated signals allowed us to  
 279 validate the chosen correction methods, both the offline and online ones. Indeed, looking at the residuals after correction in Figure 9, one can see that  
 280  
 281

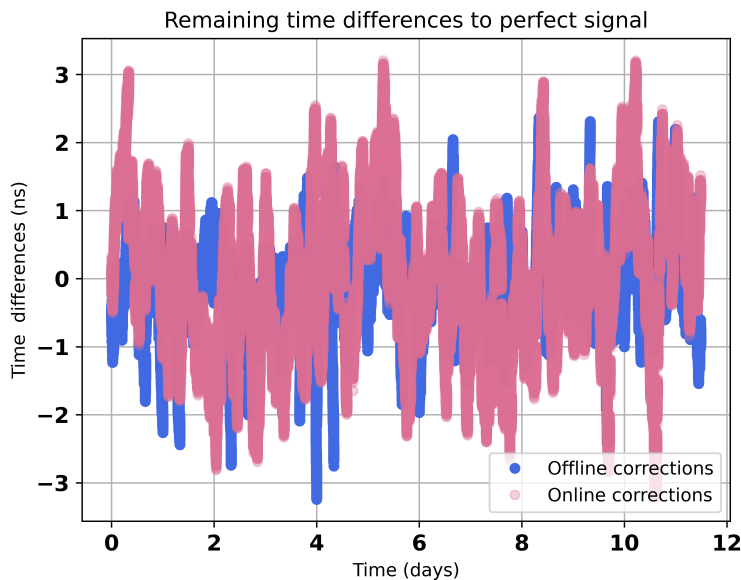


Figure 9: Comparison of time variations for simulated signals corrected with the offline method (blue) or with the sliding interval online method (pink)

282 the remaining variations for both methods are well within the experimen-  
 283 tal requirements as they stay within a few ns. Seven different simulations  
 284 were produced to take into account statistical fluctuations and the remaining  
 285 time variations were found to be for offline and online corrections respectively  
 286  $\sigma_{Off} = 0.64 \pm 0.06$  ns and  $\sigma_{On} = 1.15 \pm 0.07$  ns.

287 Finally, it is important to note that although this validates the methods for  
 288 application on data, those are simplified simulations, in particular because  
 289 only the two noise types are taken into account. As a result, we do expect  
 290 differences of performance of the correction on real data. It is also possible  
 291 that the optimal time window for the correction is slightly different for real  
 292 data because the simulations are not exact representation of data. Two main  
 293 differences can be noted: the absence of **frequency drift** and flicker noises in  
 294 the simulated Rubidium signal and the fact that we assume a perfect signal  
 295 to compare the Rubidium signal to when evaluating the OASD. **Note that the**  
 296 **frequency drift induces a quadratic drift of time signals and should therefore**  
 297 **be automatically corrected by our correction method.**



298 *2.2.3. Implementation on data*

299 To check the impact of the correction we compare the Rubidium clock  
300 signal before and after correction to the UTC(OP) that we receive at the  
301 laboratory via the T-REFIMEVE network. The UTC(OP) time signal plays  
302 the role of the perfect signal used for the simulations, while obviously not  
303 being perfect. This first difference is to take into account while comparing  
304 performances on simulated data to performance on experimental data. In  
305 the following, we will quantify the stability of the Rubidium signal using  
306 the OASD of a time series (according to equation (10) of [31]) consisting of  
307 time differences between this signal and the UTC(OP). Measuring this time  
308 difference frequently, once per second for instance, will allow to also evaluate  
309 the very short term stability of the corrected signal which is not possible with  
310 the Septentrio measurements that are integrated over 16 minutes. We use  
311 the counter to provide such a measurement every 1 second approximately.  
312 We then perform a simultaneous correction of the Rubidium - GPS Time,  
313 as measured by the Septentrio receiver, and of this measured time series.  
314 Comparing the OASD of the corrected time series to the uncorrected one,  
315 one can quantify the short term stability (below 16 minutes) after correction  
316 while making sure that the random walk was corrected. We can also use this  
317 comparison to optimize the value of  $\Delta t$  in order to achieve the lowest Allan  
318 Standard Deviation possible at all averaging time.

319 **3. Results**

320 In this Section, we present the results of the correction of the Rubidium  
321 clock time stamps obtained for simultaneous measurements of around 35  
322 days with the Septentrio receiver and the counter. The OASD of the time  
323 series measured by the counter is shown in Figure 6. Note that the statistical  
324 uncertainty on the estimated OASD, due to the limited number of samples  
325 per averaging time, are included as error bars for both curves (Rb and GPS)  
326 but they are too small to be visible. Indeed for the Rb vs UTC(OP) OASD,  
327 the statistical uncertainty is at the permil level. Up to an averaging time of  
328 around  $4 \cdot 10^3$  s, the stability is limited only by the phase white noise and then  
329 by the frequency white noise. After that, the OASD first increases as  $\tau^{1/2}$   
330 which is characteristic of the frequency random walk. From  $\tau \approx 7 \times 10^4$  s, the  
331 OASD increases proportionally to  $\tau$ . This is characteristic of a deterministic  
332 frequency drift which can be easily characterized and corrected for contrary  
333 to the frequency random walk. In comparison, the OASD of the difference

334 between GPS Time and the UTC(OP) reference PPS signal that we receive  
335 from LNE-SYRTE, is only limited by a phase white noise at least up to an  
336 averaging time of  $5 \times 10^5$  s: the OASD keeps decreasing with the averaging  
337 time. At low averaging times, the GPS stability is worse than that of the Rb  
338 because of this phase white noise: the GPS OASD is of around  $3 \times 10^{-12}$  at  
339 960 s compared to around  $2 \times 10^{-13}$  OASD for the Rubidium clock. However,  
340 at around  $10^4$  s, the stability of the Rb signal becomes worse compared to  
341 GPS Time because of the frequency random walk and drift of the Rubidium  
342 clock.

343 In this paper, we used only the GPS satellites with an elevation angle (an-  
344 gles between line of sight and horizontal direction) larger than  $15^\circ$  to extract  
345 the Rubidium time residuals distribution. During the whole data-taking pe-  
346 riod, for each data point, the Septentrio receiver was able to track an average  
347 of 6.5 GPS satellites and at least 4 GPS satellites for each data point. To  
348 obtain the Rubidium vs GPS Time difference, we take the mean value of the  
349 differences between the Rubidium clock and each GPS satellite tracked in  
350 the same integration time window of the Septentrio receiver. The obtained  
351 time difference is shown in Figure 10. **It shows that the Rubidium clock time  
352 signal drifts away from the GPS Time in a quadratic function of time because  
353 of the frequency linear drift. After around 35 days, the difference surpasses  
354  $25 \mu\text{s}$ . A zoom on the first five days of data also shows some shorter term  
355 fluctuations characteristic of the frequency random walk. Because of those  
356 two sources of frequency drift, we see that after a few days of data-taking,  
357 the Rubidium clock time signal can drift away from the GPS Time by more  
358 than a hundred nanoseconds.**

### 359 *3.1. Offline correction*

360 Figure 11 shows the Allan Standard Deviation of the Rubidium-UTC(OP)  
361 data. **Note that the measurement rate of the counter was of around 0.995  
362 measurement per second.** The blue curve shows the result for the raw series,  
363 before any correction. The other colored curves show the results for the  
364 series corrected offline, with different width of the correction time window.  
365 Here, we use quadratic fits of the Septentrio data (so  $a_k \neq 0$  a priori). The  
366 shortest time window (2880 s) corresponds to approximately 3 Septentrio 16  
367 minutes epochs. The medium (10560 s) and largest (240,000 s) correspond  
368 respectively to 11 and 250 Septentrio data points.

369 One sees that with the medium time window compared to the two others,  
370 we obtain the best stability at all averaging times. At lower averaging times,

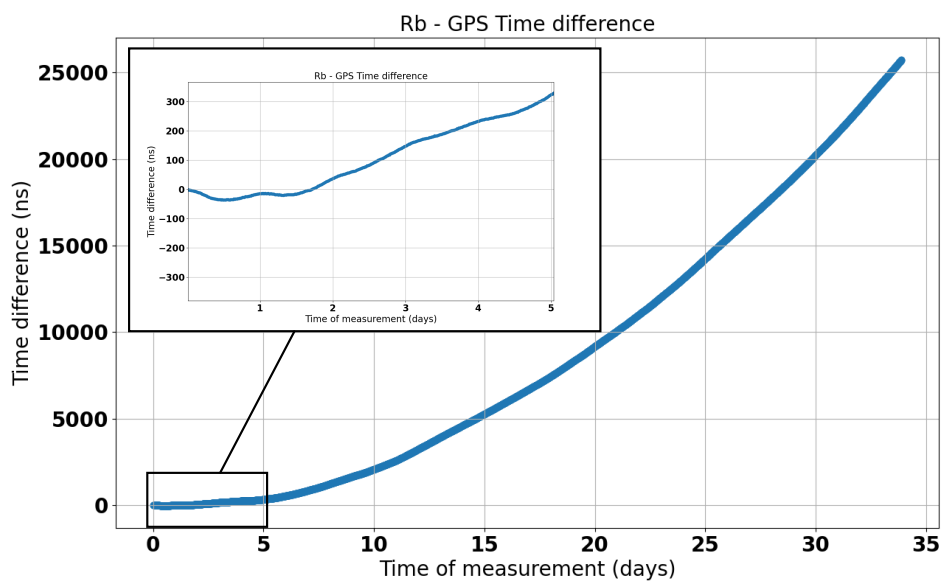


Figure 10: Time difference between the Rubidium clock and GPS Time as measured by the Septentrio receiver. The long term quadratic drift is due to the linear frequency drift of the clock. The zoom on the first five days of data also shows shorter term fluctuations caused by the frequency random walk of the Rubidium clock.

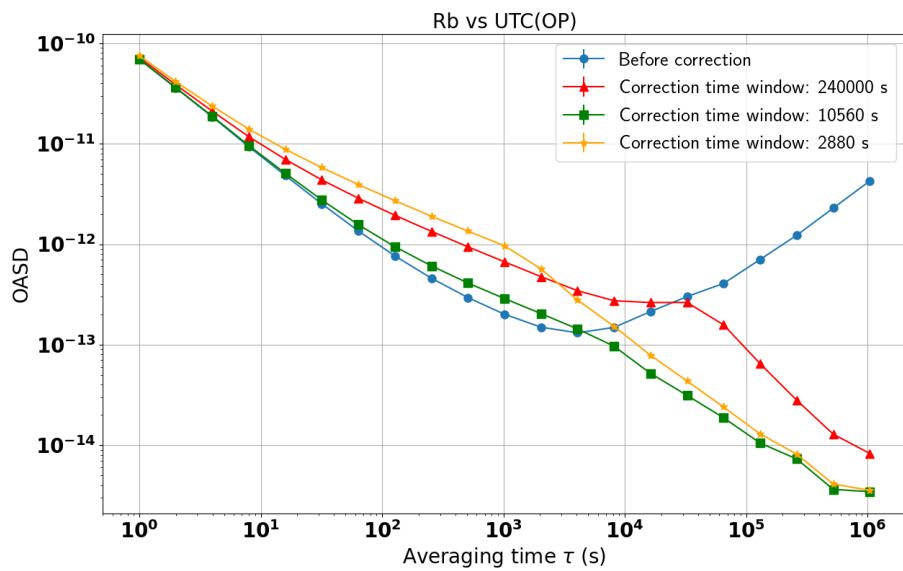


Figure 11: Overlapping Allan Standard Deviation of the Rb - UTC(OP) time series before correction (in blue) and after the correction with a correction time window of 2880 s (orange), 10560 s (green) and 240,000 s (red). The best stability at both short and long averaging times is obtained for the medium time window (10560 s  $\approx$  3 hours).

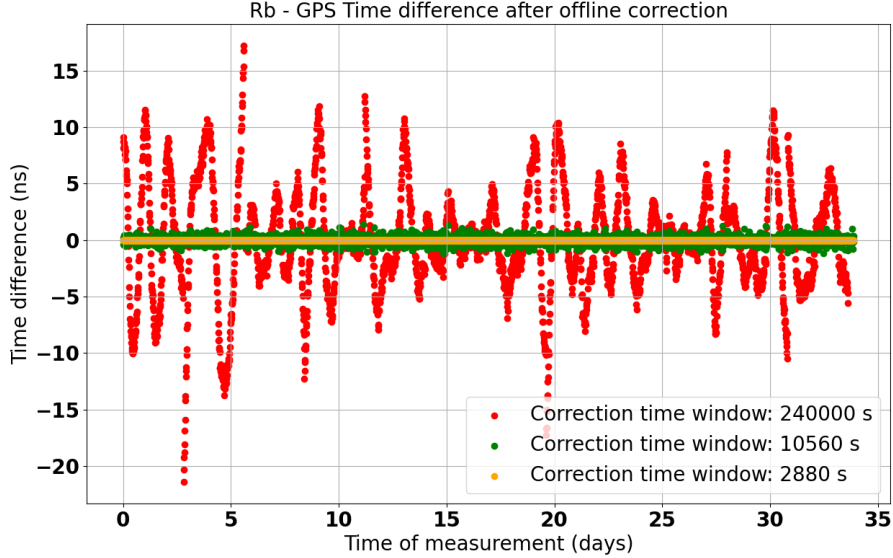


Figure 12: Time difference between the Rubidium clock and GPS Time after the offline correction. Three different correction time windows have been tested: 2800 s (orange), 10560 s (green) and 240,000 s (red). These residuals can be compared to the time difference before correction that were shown in Figure 10.

371 the performance is very similar to the uncorrected time series. At higher  
 372 averaging times, the Allan Standard Deviation is much better than the un-  
 373 corrected series as it keeps decreasing with increasing  $\tau$ . This is also the  
 374 case for correction with the shortest time window. This illustrates the fact  
 375 that both the 2880 s and 10560 s windows are able to correct the frequency  
 376 random walk and linear drift of the uncorrected time series. However, with  
 377 the shortest correction time window, the short term stability of the time se-  
 378 ries is degraded compared to the uncorrected series: the value of the ASD at  
 379 100 s increases by a factor 3. In this scenario, the corrected Rubidium time  
 380 signal gets very close to GPS Time which is known to have a higher phase  
 381 White Noise. Finally, the longest correction time window leads to a similar  
 382 stability as the shortest one for a small  $\tau$ , and poorer stability at large  $\tau$   
 383 (above  $5 \cdot 10^3$  s).

384 Figure 12 shows the Rubidium vs GPS Time difference after the offline  
 385 correction. In offline mode, the shorter the correction time window, the lower  
 386 the residual differences. However, with the medium length time window, we

387 still get time residuals lower than 3 ns over the whole data-taking period,  
388 which is well below the requirements of HK. With the longest correction  
389 time window, jumps of a few tens of nanoseconds are introduced in the time  
390 residuals. This explains the overall higher ASD: the stability of the signal is  
391 limited by those jumps. The time scale of the variations in the data to fit  
392 is too small compared to the 240,000 s time window. In consequence, the  
393 fitted tendency from one piece to another is very different, and the fitted  
394 piece-wise polynomial is not continuous. **It is also interesting, as a cross-**  
395 **check, to have a look at the fluctuations in the time difference between the**  
396 **Rubidium clock and the UTC(OP) after correction. This is summarized in**  
397 **the first line of Table 2 that gives the standard deviation of the time series**  
398 **after correction. The deviations with the two shorter correction time windows**  
399 **are indeed very small (below 2 ns) confirming that this method can be used**  
400 **for synchronization to UTC.**

401 With the offline version of the corrections, we thus obtain a very good  
402 synchronization to GPS Time at the level of a few nanoseconds with the  
403 10560 s time window. However, this version of the correction cannot be  
404 applied in real time. In the following, we show the results for the online  
405 version of the correction that can be applied in real time to correct the time  
406 stamps of events in physics experiments.

### 407 3.2. Online correction

408 Figure 13 shows the Allan Standard Deviation of the uncorrected (blue)  
409 and online corrected (other colors) Rubidium - UTC(OP) times series. The  
410 same three correction time windows intervals as before are considered. The  
411 top panel shows the results using quadratic fits of the Septentrio data and  
412 the bottom panel shows the results with linear fits. For the shortest and  
413 medium correction time windows, the linear fits lead to better performance  
414 with a lower OASD at low averaging times. At 1000 s, the OASD with the  
415 shortest (medium) correction time window is reduced by a factor 2 to 3 (resp.  
416 1.5).

417 This behavior can be understood by looking at the number of degrees of  
418 freedom (number of data points - number of free parameters) in our fits. For  
419 the shortest time windows, the number of degrees of freedom is relatively  
420 low (0 and 8) in case of quadratic fits so we risk over-fitting to the past  
421 data in order to correct the present data. This number of degrees of freedom  
422 is less relevant in the offline correction as the fit is performed on the same  
423 data as the correction (the over-fitting is not a problem here). Lowering the

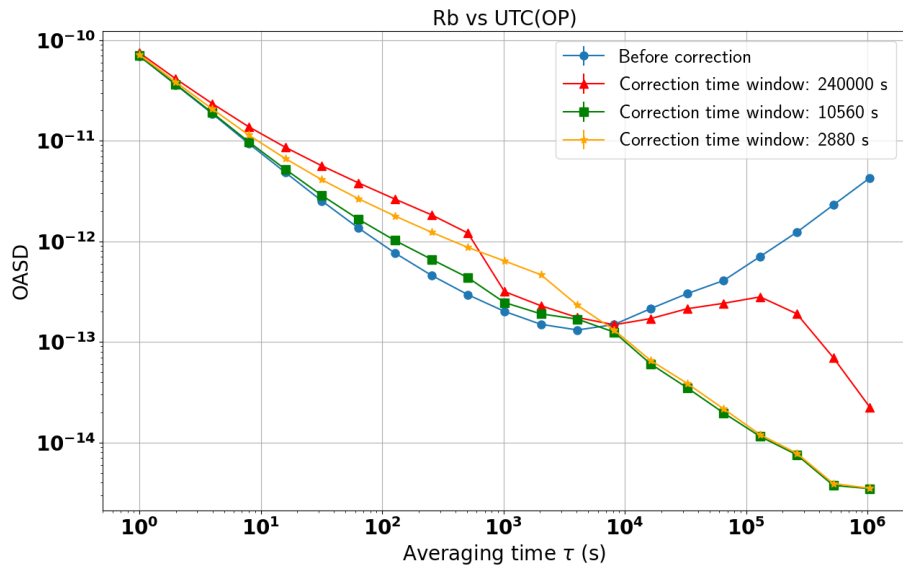
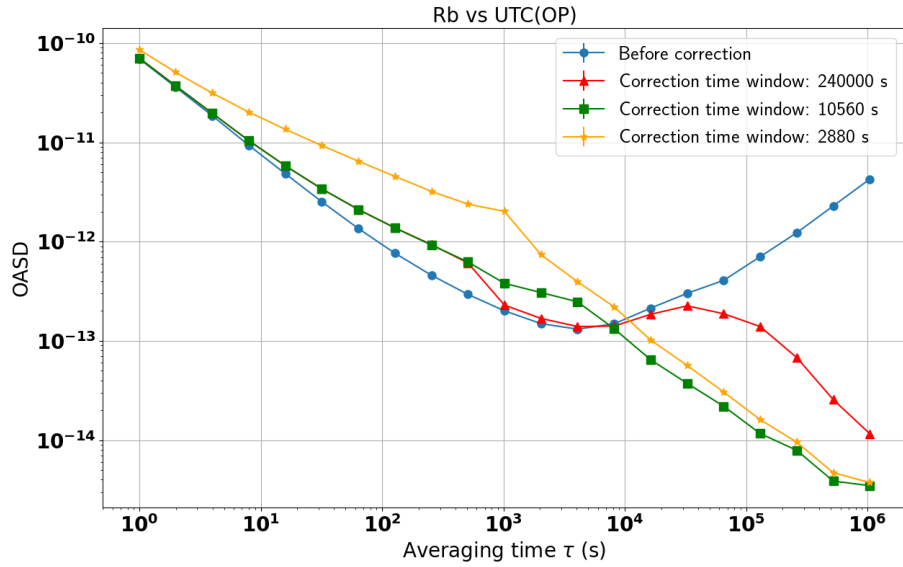


Figure 13: Overlapping Allan Standard Deviation of the Rb - UTC(OP) time series before correction (in blue) and after the online correction with a correction time window of 2880 s (orange), 10560 s (green) and 240,000 s (red). The data were fitted with quadratic (top) or linear (bottom) functions of time. A better stability, similar to the offline correction, can be obtained using linear fits.

424 number of free parameters is one way of increasing the degrees of freedom  
425 hence allowing the fit to better generalize to the present data. Another way  
426 to increase the number of degrees of freedom is to increase the number of  
427 data points in the fit. For the longest time window, there are 247 degrees  
428 of freedom in the quadratic fit so we lower the risk of over-fitting. On the  
429 contrary, in that case, quadratic fits lead to a slightly better correction of  
430 the random walk that limits the stability only up to  $\tau \sim 3 \times 10^4$  s whereas  
431 with linear fits, it limits the stability up to  $\sim 10^5$  s. Note that, especially  
432 for the shortest correction time window we see a clear degradation of the  
433 stability for averaging times lower than the correction window's length. This  
434 is a known effect from linear servo loop theories and periodic perturbations  
435 of oscillators [32] and it could be attenuated by scaling down the correction:  
436 instead of subtracting the result of the fit, we could subtract only a fraction  
437 of it.

438 Regarding the stability of the corrected Rubidium clock, using linear fits,  
439 the conclusions are the same as for the offline correction. The lowest Allan  
440 Standard Deviation, for all averaging times, is achieved with the medium  
441 width correction time window. With the shortest time window, the short  
442 term stability is degraded, and with the longest correction time window, we  
443 find poorer long term stability compared to the other corrected scenarios.

444 If the correction time window is too wide, we cannot correct as well the  
445 frequency random walk of the free-running Rubidium: the risk is that the  
446 Rubidium time signal locally drifts too far away from the GPS Time. This  
447 can be observed in the corrected Rubidium against GPS Time in Figure 14  
448 where the maximum difference reaches around 80 ns (or 25 ns with quadratic  
449 fits) with the 240,000 s correction time window. With the 10560 s correc-  
450 tion time window, the differences stay in the  $\pm 5$  ns range. **The standard  
451 deviation of the time difference with the UTC(OP) is also shown in Table  
452 2 for both online corrections. Once again, one can see the reduction of the  
453 white noise when using linear instead of quadratic fits.** Before correction,  
454 as the reader saw in Figure 10, the free-running Rubidium clock can drift  
455 away from the GPS Time by around 100 ns in less than 3 days which means  
456 that HK's requirement for the synchronization with UTC is not met. After  
457 online correction with the longest time window tested, the corrected Rubid-  
458 ium time stamps drift by around 60 ns in a few days because of remaining  
459 random walk noise. Even though during the 35 days data-taking period the  
460 time residuals with respect to GPS Time does not exceed 100 ns, it is not  
461 possible to safely claim that the Rubidium clock drift will not exceed HK's



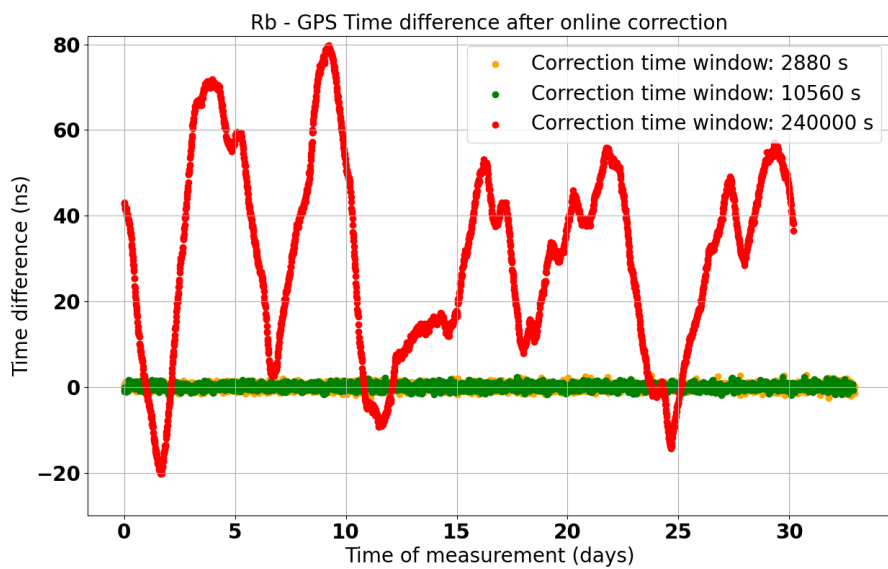
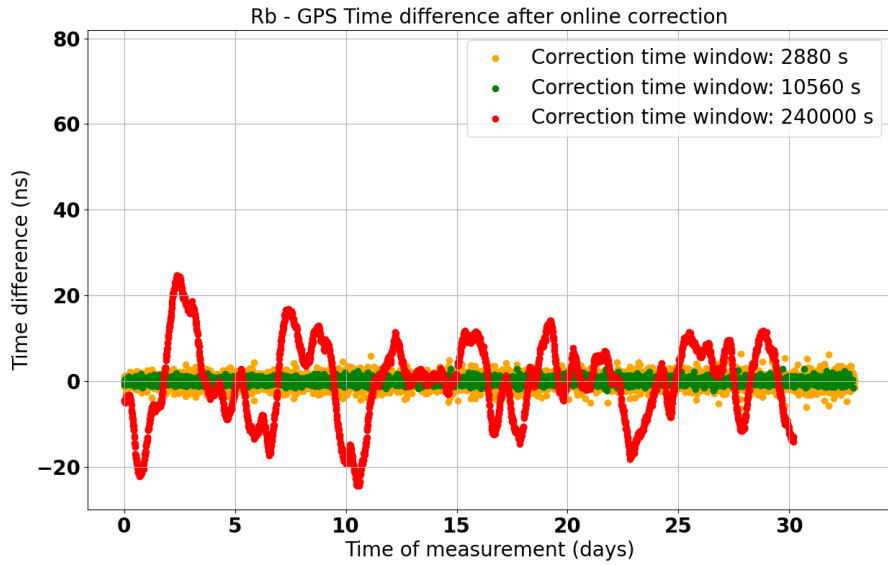


Figure 14: Time difference between the Rubidium clock and GPS Time after the online correction. Each point is corrected using a quadratic (top) or linear (bottom) fit of the 2800 s (orange) or 10560 s (green) or 240,000 s (red) of data points prior to this point. Using linear fits leads to smaller residuals for the shortest time window and bigger ones for the longest time window.

correction time window	2880 s	10560 s	240000 s
offline correction	1.87 ns	1.79 ns	5.13 ns
online correction (quadratic fits)	2.01 ns	1.83 ns	9.35 ns
online correction (linear fits)	1.84 ns	1.81 ns	22.66 ns

Table 2: Standard deviation of the time difference between the Rubidium clock PPS signal and the UTC(OP) after correction.

462 requirement of 100 ns if we use the 240,000 s correction time window, be-  
463 cause of the random nature of this drift. With shorter time windows, no  
464 residual drift is observed, and the residuals are thus contained in a range of  
465 a few nanoseconds.

#### 466 4. Discussion

467 As advertised before, the advantage of the so-called online correction is  
468 that it could be performed in real-time. This is an important feature for  
469 applications that necessitate a real-time synchronization with UTC or with  
470 another site (like the future HK or DUNE experiments). If a reference clock  
471 signal is generated with an atomic clock (like the Rubidium clock used here)  
472 and sent to a data acquisition system to be propagated to detectors and pro-  
473 vide time stamps, one could continuously compare this signal to GPS Time  
474 using a Septentrio receiver. The correction coefficients  $a$ ,  $b$  and  $c$  calculated  
475 from the Septentrio data would need to be sent to the data acquisition system  
476 so that it could correct the time stamps in real-time.

477 Figure 15 shows the standard deviation of the Rb vs GPS Time differ-  
478 ence after correction as a function of the correction time window's width. The  
479 performance of the offline and online corrections on experimental data (col-  
480 ored dots) are compared to the performance we had obtained on simulated  
481 data (colored triangles) with a correction time window of 2880 s, 28800 s and  
482 240000 s. Note that these simulated data were only taking into account phase  
483 white noise, frequency white noise and frequency random walk components.  
484 **In particular, the measured data also contain a linear frequency drift and**  
485 **this main difference could partly explain the difference of performances ob-**  
486 **erved between data and simulation.** Also, no additional uncertainties were  
487 added to take into account other types of noise (e.g: flicker noise) or exper-  
488 imental conditions (e.g: imperfect calibrations, etc.). For both corrections,  
489 very similar performance of synchronization with GPS Time are obtained for

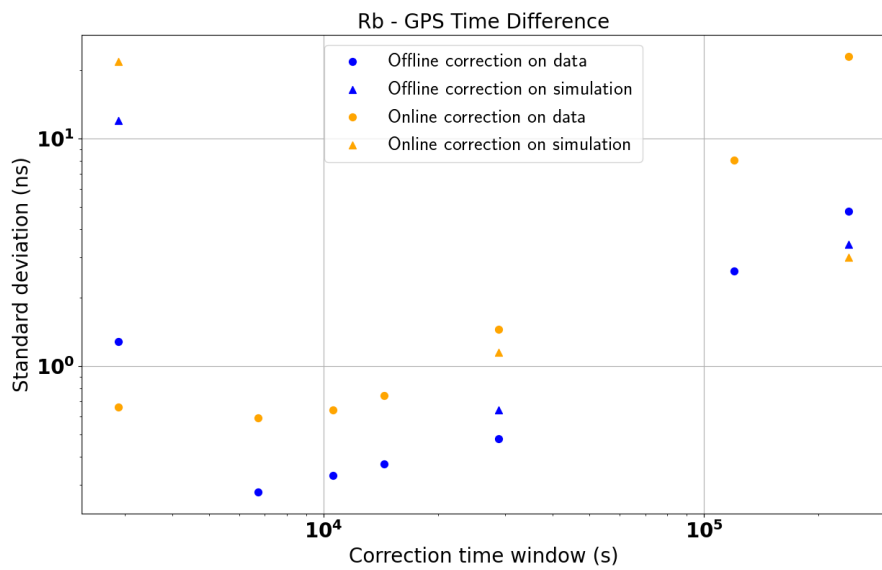


Figure 15: Standard deviation of the residuals distributions between the Rb and the GPS Time after the offline (blue) or online (orange) correction as a function of the correction time window. Quadratic fits of the Septentrio data are used for the offline correction whereas linear fits are used for the online correction. The performance on simulated data is also shown for three values of the correction time windows.

490 correction time windows below 30,000 s so there is no need to have much  
491 shorter windows. This result is consistent with the fact that, as seen in Fig-  
492 ure 6, the stability of the Rubidium signal becomes worse than that of the  
493 GPS around  $10^4$  s. The offline correction seems to provide a slightly better  
494 synchronization to GPS Time (down to  $\sim 0.3$  ns **update**) but the precision  
495 achievable with the online correction is already more than satisfying: better  
496 than 5 ns for correction time windows below 100,000 s.

## 497 5. Conclusions

498 In this paper, we presented a simple way to use time comparisons to  
499 GPS Time to synchronize the time stamps, generated using a free-running  
500 Rubidium clock, close to UTC while preserving its short term stability and  
501 correcting for the long term frequency random walk **and deterministic drift**.  
502 This method has the advantage of using relatively cheap instruments and to  
503 be applicable online for a real-time synchronization as well as to be robust  
504 against punctual GPS signal reception failures. The online method could  
505 be applied for the real-time synchronization between several experimental  
506 sites in long-baseline accelerator neutrino experiments as well as for other  
507 detectors involved in multi-messenger astrophysics measurements.

508 The proposed method consists in fitting the GPS Time vs Rubidium mea-  
509 sured by a GNSS receiver with a piece-wise polynomial function of time and  
510 in subtracting the result to the generated time stamps. The method was  
511 first designed and validated with simulated signals before assessing its per-  
512 formance on real data. We evaluated the performance of this correction by  
513 quantifying the stability of the clock signal before and after the correction  
514 using the Overlapping Allan Standard Deviation. We showed that the op-  
515 timal length of the time window for the fit of the GPS Time vs Rubidium  
516 seats around 10,000 seconds, corresponding to around 10 data points from  
517 the receiver. This time window allowed to maintain the best possible short  
518 term stability while correcting efficiently the frequency random walk. After  
519 correction with this time window, the difference to GPS Time stays within  
520 a window of  $\pm 5$  ns for both offline and online corrections during the whole  
521 period of 35 days of measurement. This performance largely meets the usual  
522 requirements for long-baseline accelerator neutrino experiments, like Hyper-  
523 Kamiokande and DUNE. Note that we do not expect the performance of the  
524 correction to be heavily degraded by isolated missing or outlier measurements  
525 from the receiver. However, this correction requires a constant monitoring

526 of the Rubidium time signal with a GNSS receiver (or other reference that  
527 can be linked to UTC). One should thus make sure that such a reference  
528 is available in the long term and that there is no risk of losing it for long  
529 periods (e.g.: several hours).

530 **Fundings:** This research was funded by IN2P3/CNRS, the French "Agence  
531 nationale pour la recherche" under grant number ANR-21-CE31-0008, the  
532 "IdEx Sorbonne Université" and the 2019 "Sorbonne Université Émergences:  
533 MULTIPLY" grant.

534 The White Rabbit network and the access of associated optical fibers to  
535 the Pierre and Marie Curie campus: T-REFIMEVE, FIRST TF and LNE:  
536 "Agence Nationale de la Recherche" (ANR-21-ESRE-0029 / ESR/Equipex T-  
537 REFIMEVE, ANR-10-LABX48-01 / Labex First-TF); Laboratoire National  
538 d'Essai (LNE), project TORTUE.

## 539 References

- 540 [1] M. Guler et al., *OPERA: An appearance experiment to search for  $\nu/\mu$   
541  $\leftrightarrow \nu/\tau$  oscillations in the CNGS beam*, Experimental proposal,  
542 CERN-SPSC-2000-028.
- 543 [2] K. Abe et al., T2K Collaboration, *The T2K Experiment*, *Nucl. In-*  
544 *strum. Meth. A* **659** (2011), 106-135, doi:10.1016/j.nima.2011.06.067,  
545 arXiv:1106.1238.
- 546 [3] D. S. Ayres et al., *The NOvA Technical Design Report*, (2007),  
547 doi:10.2172/935497.
- 548 [4] K. Abe et al., *Hyper-Kamiokande Proto-Collaboration*, *Hyper-*  
549 *Kamiokande Design Report*, (2018), arXiv:1805.04163.
- 550 [5] B. Abi et al., *Deep Underground Neutrino Experiment (DUNE), Far*  
551 *Detector Technical Design Report, Volume I: Introduction to DUNE*,  
552 (2020), arXiv:2002.02967.
- 553 [6] D. Cussans et al., *Timing and synchronization of the DUNE neutrino*  
554 *detector*, *Nuclear Instruments and Methods in Physics Research, A* **958**  
555 (2020), doi:10.1016/j.nima.2019.04.097.

- 556 [7] P. Mészáros, D.B. Fox, C. Hanna et al., *Multi-messenger astrophysics*,  
557 *Nat. Rev. Phys.* **1** (2019) 585–599, [https://doi.org/10.1038/s42254-019-](https://doi.org/10.1038/s42254-019-0101-z)  
558 0101-z.
- 559 [8] The Supernova Early Warning System web page, <https://snews2.org/>.
- 560 [9] K. Abe et al., T2K collaboration, *Upper bound on neutrino*  
561 *mass based on T2K neutrino timing measurements*, *Physical Re-*  
562 *view D* **93** (2016) 1, 012006, doi: 10.1103/PhysRevD.93.012006,  
563 <https://arxiv.org/abs/1502.06605>.
- 564 [10] Y. Fukuda et al., Super-Kamiokande collaboration, *The Super-*  
565 *Kamiokande detector*, *Nucl.Instrum.Meth.A* **501** (2003) 418,  
566 [https://doi.org/10.1016/S0168-9002\(03\)00425-X](https://doi.org/10.1016/S0168-9002(03)00425-X).
- 567 [11] L. Mellet, M. Guigue, B. Popov, S. Russo, V. Voisin, on behalf of the  
568 Hyper-Kamiokande Collaboration, *Development of a Clock Generation*  
569 *and Time Distribution System for Hyper-Kamiokande*, *Phys. Sci. Forum*  
570 **8** (2023) 72, <https://doi.org/10.3390/psf2023008072>.
- 571 [12] M. Lombardi, *Fundamentals of Time and Frequency*, *The Mechatronics*  
572 *Handbook*, CRC Press: Boca Raton, FL, USA (2002), ISBN 978-0-8493-  
573 6358-0.
- 574 [13] Giulia Brunetti, *Neutrino velocity measurement with the OPERA exper-*  
575 *iment in the CNGS beam*, Université Claude Bernard - Lyon I; Univer-  
576 sità degli studi (Bologne, Italie), 2011. English. ⟨NNT : 2011LYO10088⟩.  
577 ⟨tel-00843100⟩
- 578 [14] M.A. Weiss, G. Petit, Z. Jiang, *A comparison of GPS common-view*  
579 *time transfer to all-in-view*, In *Proceedings of the IEEE International*  
580 *Frequency Control Symposium and Exposition*, 2005.
- 581 [15] The National Institute of Information and Communications Technology  
582 (NICT), Japan. <https://www.nict.go.jp/en/>
- 583 [16] <https://www.bipm.org/en/time-ftp/circular-t>
- 584 [17] J. Serrano et al., *The White Rabbit project* (2013),  
585 <https://cds.cern.ch/record/1743073>.

- 586 [18] E. Cantin et al., *REFIMEVE Fiber Network for Time and Frequency*  
587 *Dissemination and Applications*, 2023 Joint Conference of the Euro-  
588 pean Frequency and Time Forum and IEEE International Frequency  
589 Control Symposium (EFTF/IFCS), Toyama, Japan, 2023, pp. 1-4, doi:  
590 10.1109/EFTF/IFCS57587.2023.10272084.
- 591 [19] C. B. Lim et al., *Extension of REFIMEVE with a White Rab-*  
592 *bit Network*, 2023 Joint Conference of the European Frequency  
593 and Time Forum and IEEE International Frequency Control  
594 Symposium (EFTF/IFCS), Toyama, Japan, 2023, pp. 1-4, doi:  
595 10.1109/EFTF/IFCS57587.2023.10272069.
- 596 [20] D.A. Howe, D.W. Allan, J.A. Barnes, *Properties of signal sources and*  
597 *measurement methods*, In Proceedings of the Thirty Fifth Annual Fre-  
598 quency Control Symposium, Philadelphia, USA, 27-29 May 1981.
- 599 [21] G. Daniluk, *White Rabbit calibration procedure (version 1.1)*  
600 (2015), [https://white-rabbit.web.cern.ch/documents/WR\\_Calibration-](https://white-rabbit.web.cern.ch/documents/WR_Calibration-v1.1-20151109.pdf)  
601 [v1.1-20151109.pdf](https://white-rabbit.web.cern.ch/documents/WR_Calibration-v1.1-20151109.pdf)
- 602 [22] G. D. Rovera et al., *UTC(OP) based on LNE-SYRTE atomic fountain*  
603 *primary frequency standards*, *Metrologia* **53** (2016) S81.
- 604 [23] <https://webapp.csr-scrs.nrcan-rncan.gc.ca/geod/tools-outils/ppp.php>
- 605 [24] P. Defraigne, G. Petit, *CGGTTS-Version 2E: an extended standard*  
606 *for GPS Time Transfer*, *Metrologia* **52** (2015), IOP Publishing, doi:  
607 10.1088/0026-1394/52/6/G1.
- 608 [25] J. Plumb et al., *Absolute calibration of a geodetic time transfer system*,  
609 *Ultrasonics, Ferroelectrics and Frequency Control, IEEE Transactions*  
610 **52** (2005) 1904-1911, doi: 10.1109/TUFFC.2005.1561658.
- 611 [26] G. D. Rovera et al., *Link calibration against receiver calibration time*  
612 *transfer uncertainty when using the Global Positioning System*, *Metrolo-*  
613 *gia* **51.5** 476490 (2014).
- 614 [27] Lucile Mellet, *From T2K to Hyper-Kamiokande : neutrino oscillation*  
615 *analysis and preparation of the time synchronization system*, PhD thesis,  
616 Sorbonne University (2023), ⟨NNT : 2023SORUS297⟩ ⟨tel-04284182⟩.

- 617 [28] J. A. Barnes et al., *Characterization of Frequency Stability*, in *IEEE*  
618 *Transactions on Instrumentation and Measurement*, vol. IM-20, no. 2,  
619 pp. 105-120, May 1971, doi: 10.1109/TIM.1971.5570702.
- 620 [29] T. J. Witt, *Using the Allan variance and power spectral density to*  
621 *characterize DC nanovoltmeters*, in *IEEE Transactions on Instrumen-*  
622 *tation and Measurement*, vol. 50, no. 2, pp. 445-448, April 2001, doi:  
623 10.1109/19.918162.
- 624 [30] D. W. Allan, *Statistics of atomic frequency standards*, in *Proceed-*  
625 *ings of the IEEE*, vol. 54, no. 2, pp. 221-230, Feb. 1966, doi:  
626 10.1109/PROC.1966.4634.
- 627 [31] W. J. Riley, *Handbook of frequency stability analysis*, *NIST* Special pub-  
628 lication 1065, July 2008.
- 629 [32] G. Santarelli, C. Audoin, A. Makdissi, P. Laurent, G. J. Dick, et A. Cla-  
630 iron, *Frequency stability degradation of an oscillator slaved to a periodi-*  
631 *cally interrogated atomic resonator*, *IEEE Transactions on Ultrasonics,*  
632 *Ferroelectrics, and Frequency Control* **45** n 4 (juill. 1998) p. 887-894,  
633 doi: 10.1109/58.710548.